Renewable Energy 99 (2016) 325–335

Contents lists available at ScienceDirect

Renewable Energy

journal homepage: www.elsevier.com/locate/renene

Estimation of Hong Kong's solar energy potential using GIS and remote sensing technologies

Man Sing Wong [a, *], Rui Zhu [a], Zhizhao Liu [a], Lin Lu [b], Jinqing Peng [b], Zhaoqin Tang [a], Chung Ho Lo [a], Wai Ki Chan [a]

[a] Department of Land Surveying and Geo-Informatics, The Hong Kong Polytechnic University, Hung Hom, Kowloon, Hong Kong
[b] Department of Building Service Engineering, The Hong Kong Polytechnic University, Hung Hom, Kowloon, Hong Kong

ARTICLE INFO

Article history:
Received 2 February 2016
Received in revised form
2 June 2016
Accepted 3 July 2016
Available online 16 July 2016

Keywords:
Building rooftop
Photovoltaic potential
Satellite imagery
Solar radiation

ABSTRACT

This paper studies the use of Remote Sensing (RS) technologies and Geographic Information Systems (GIS) for estimation of city-wide photovoltaic (PV) potential in Hong Kong. It investigates the spatial distribution of cloud coverage through geostationary satellites from the Multi-functional Transport Satellite (MTSAT). The results indicate that a non-prominent spatial variation of cloud cover presides over a majority of Hong Kong territories. Appropriate locations for deploying solar PV panels, such as rooftops, were delineated using RS, GIS, and existing ancillary data. Extraction and filtering of pixels based on a set of criterions were used to identify optimal PV rooftops. This study shows that the summarization of PV potentials in Hong Kong is 2.66 TWh on building rooftops. The methodologies and findings from this study permits detailed spatial estimation of city-wide solar energy potential, and assists the policy-decision process on the use of renewable energy in Hong Kong.

1. Introduction

Energy consumption in a metropolitan city such as Hong Kong is extremely high, with approximate electricity consumption of 155,079 TJ; oil & coal products consumption of 83,275 TJ; town Gas & LPG consumption of 49,616 TJ in 2012 [1]. Emissions of the anthropogenic greenhouse gas have increased since than ever [2] due to the rapid economic and population growth. In Hong Kong, about 97% of total carbon dioxide emissions resulted from electricity generation [3,4]. The greenhouse gases are the major causative factors in global warming, which accelerate the insulating effect in the atmosphere. The mitigation of climate change then becomes predominant in public awareness.

Using renewable energy is one of the approaches to mitigate the greenhouse effect. Solar photovoltaic (PV) technology is a widely adaptable application and converts the solar energy into electricity with promising efficiencies [5]. The major types of renewable energy that are currently available in Hong Kong includes: solar energy, wind energy, bio-gas, and bio-diesel fuel. However, the amount of renewable energy outputs only accounts for 0.1% of the total electricity consumption. The solar energy contributes about 1.5% of total renewable energy usage in 2012 [4]. To enhance the development of solar renewable energy in Hong Kong and increase the rate of PV deployments, a study of the potential of developing solar photovoltaic energy in Hong Kong is urgently needed. The estimation of rooftop PV potential provides fundamental data for future energy policy decision-making, urban sustainable development, and city planning by the Government of Hong Kong Special Administrative Region (HKSAR). The PV potential is deemed as the annual potential energy produced from PV technology in this study.

Solar radiation is a controlling factor in electricity generation of a PV system because of the complex energy interactions between the atmosphere and surface [6]. The amount of incident solar radiation affects the electricity produced by PV systems significantly. The energy of solar radiation varies greatly due to the refraction and scattering of aerosols, water vapour contents, and air particulates. At the global scale, the geometry of the Earth and its rotation determine the latitudinal gradient radiation. At the local scale, the solar radiation map depends on the surface terrain [6]. The variations in elevation, slope, aspect, and shadowing effects cause significant deviations of solar radiation [7]. Different methods can be

* Corresponding author.
E-mail addresses: lswong@polyu.edu.hk (M.S. Wong), r.zhu@connect.polyu.hk (R. Zhu), george.liu@polyu.edu.hk (Z. Liu), vivien.lu@polyu.edu.hk (L. Lu), jallenpeng@gmail.com (J. Peng), zhaoqian.tang@connect.polyu.hk (Z. Tang), lo.chungho@connect.polyu.hk (C.H. Lo), waikiedward.chan@connect.polyu.hk (W.K. Chan).

http://dx.doi.org/10.1016/j.renene.2016.07.003
0960-1481/

used to estimate solar radiation according to the required scale and accuracy.

Variations in elevation gradient, together with shadowing effect, can cause significant local irradiance fluctuations [8]. In order to improve the spatial resolution and thematic accuracy of the solar radiation map, high resolution data derived from airborne Light Detection and Ranging (LiDAR) technology have also been used in recent studies [9–11]. LiDAR technology is used to measure the distances between sensor and objects by illuminating with a laser beam. The point cloud processes from LiDAR data such as extraction, segmentation, and reconstruction of building rooftops for solar photovoltaic deployment have been studied [9,10]. Research such as that of Nguyen et al. [11] studied the solar photovoltaic potential by considering many influential factors (e.g. terrain and near ground shadowing effects), however the weather conditions have not been considered. The solar radiation model integrated with Geographical Information Systems provides a means for proper estimation [11]. The solar radiation model is a physical model, empirical equations are adopted in order to provide fast and accurate estimation of solar radiation. It also considers the effect of slope, aspect, and shadow from the surrounding environment. Several GIS-based solar radiation models have been developed such as SolarFlux, which simulates the shadow patterns by direction insolation at specified time intervals [12], or the Solei model, which is a standalone model that works together with GIS software IDRISI [13]. Both SolarFlux and Solei use simple empirical formulas [14] and parameters represented by generalized values, which implies that they may not be suitable for an accurate estimation for a large region. Solar Analyst is an extension module of ArcGIS [15], which derives solar radiation map based on the input DSM and DEM data [16,17]. Several other factors are also considered during the process such as slope, aspect, solar angle, shadow casting by surrounding topography, and atmospheric attenuation [9]. For the calculation of diffuse proportion and atmospheric transmissivity, the parameters input into the Solar Analyst can be in reference to the nearest meteorological station data or typical default values [11]. Another solar radiation model, the SRAD model, simulates the interactions between longwave and shortwave solar radiation with the Earth's surface and its atmosphere. The main solar radiation factors are considered for the spatial variability of landscape processes based on a simplified parameterization [6]. However, it is designed for analyzing the topographical and meso-scale process, thus the estimation over large areas may not be appropriate.

In this study, Solar Analyst was selected to estimate the solar radiation of unused areas on rooftops. The input data for solar radiation calculations are DSM and DEM generated from airborne LiDAR data. The incoming solar radiation received from the sun is the primary energy source, containing two main parts: direct radiation which is intercepted and unimpeded, and diffuse radiation which is scattered by atmospheric constituents such as clouds and aerosols.

The objectives of this study are: (i) to analyze the spatial distribution of possible cloud covers in Hong Kong; (ii) to develop a robust method for estimating annual solar potential in areas of unused building rooftops; and (iii) to further validate the results from solar radiation modeling with ground-based observation. The methodologies and findings from this study can enable detailed spatial estimations of city-wide solar energy potential, where the generated potential energy can be fed back into the grid and/or be used directly in households/offices consumption.

This paper is organized as follows: Section 2 outlines the descriptions of the study area and data used, Section 3 presents the derivation of cloud probability map, Section 4 describes the method for estimating solar potentials in areas of unused rooftops, and Section 5 summarizes the major findings, limitations and conclusions.

2. Study area and data used

Hong Kong, located on 22° latitude with a sub-tropical climate, has more than 7 million population with an average population density of 6544 per km^2 [18], which consumed 153,362 TJ electricity in 2013 [19]. The Hong Kong area covers Hong Kong Island, Lantau Island, Kowloon Peninsula, and the New Territories, including 262 outlying islands. The urban landscape as known by many, comprising of high-rise buildings for both commercial and residential purposes, occupies around 8% of Hong Kong's land area. However, 90% of Hong Kong's electricity consumption comes from these buildings.

2.1. Satellite data

In order to derive a cloud cover probability map for Hong Kong, a year's worth of Multi-functional Transport Satellite images (MTSAT-1R/MTSAT-2) were acquired for the year of 2012 and used in this study. The images cover the Earth's surface from 5° N to 55° N and from 75° E to 145° E with an hourly-based temporal resolution. The acquired data are then post-processed at a 4 km spatial resolution for both visible and infrared channels, where the original resolutions are 1 km and 4 km respectively. All MTSAT image files are stored in HDF-4 format, consisting of seven data layers: VIS, IR1, IR2, IR3, IR4, Latitude, and Longitude.

2.2. Elevation data - Hong Kong DSM and DEM

The Digital Surface Model (DSM) and Digital Elevation Model (DEM) data were generated by the airborne LiDAR point cloud data and stored as raster format. The data acquisition was carried out for the entire Hong Kong territory by the Civil Engineering and Developing Department (CEDD) of Hong Kong SAR Government using airborne laser scanner observation between December 2010 and January 2011. The average point spacing is 0.5 m (4 pt/m^2) and the horizontal and vertical accuracies are 0.3 m and 0.1 m respectively [20].

2.3. Hong Kong building GIS data

The GIS data for building footprints in Hong Kong are in polygon shapefile format. Each polygon represents the corresponding building in an object space. The corresponding attribute table for each polygon contains a list of attributes including: area, georeference number, and building names. GIS data were used to extract building outlines and building pixels, and later exported to the solar potential calculation of individual buildings.

2.4. Hong Kong weather data

The weather data of 2012, including the cloud cover data, can be retrieved from the website of Hong Kong Observatory [21].

3. Derivation of cloud probability map

This section illustrates the method for the derivation of cloud probability map using geostationary satellite images in Hong Kong.

3.1. Calculation of solar and satellite angles

For the image pre-processing, solar and satellite view angles are critical for determining day-time observation and in the use of radiative transfer model for determining the cloud thresholds. The

geostationary MTSAT satellite images consist of latitude and longitude information of each pixel, and metadata describing the satellite orbital information. These data enable calculation of the instantaneous satellite viewing geometry. Solar geometry and viewing geometry are composed of several angles: solar zenith angle θ_{sun} (SZA); satellite zenith angle θ_{sat} (also known as viewing zenith angle, VZA); and the difference angle between solar azimuth angle (α_{sun}) and satellite azimuth angle (α_{sat}), known as relative azimuth, represented as α_{rel}. Estimated angles in this section were used as inputs in the radiative transfer model. If the calculated solar zenith angle is larger than 90°, it is then defined as night-time observation.

3.2. Radiative transfer model

Radiative transfer model is used to calculate radiance of the Earth's atmosphere at different wavelengths under different atmospheric and surface conditions. The radiances at the top of the atmosphere (TOA) measured by satellite sensors are influenced by atmospheric scattering and surface reflected solar radiance. In this study, atmospheric parameters retrieved from satellite images together with other climatology and ancillary data were used as inputs in radiative transfer model to simulate the cloud-free TOA apparent reflectance for MTSAT visible wavelength. The simulation was conducted using the "Second Simulation of the Satellite Signal in the Solar Spectrum" (6S) radiative transfer model [22].

The 6S model is a fundamental radiative transfer code used for the calculation of look-up tables in atmospheric correction. For a Lambertian surface, the TOA apparent reflectance ρ_{TOA} can be calculated using Equation (1):

$$\rho_{TOA}(\theta_{sun},\theta_{sat},\alpha_{rel}) = \rho_a(\theta_{sun},\theta_{sat},\alpha_{rel}) + \frac{\rho_t}{1-\rho_t S}T(\theta_{sun})T(\theta_{sat}) \quad (1)$$

where ρ_a is path reflectance (caused by Rayleigh scattering and aerosol scattering) without surface contribution, ρ_t is the surface reflectance, S is the spherical albedo of the atmosphere, and $T(\theta_{sun})$ $T(\theta_{sat})$ is the total transmittance. For this study, land areas with surface properties of grass, forest, and barren land were assumed as land cover types. Over ocean areas, the reflectance values of lake water properties were defined in the 6S model isotropy.

In order to reduce the computational workload and time, "Look Up Tables" (LUTs) were developed for various discrete atmospheric and solar satellite viewing geometry. The mid-latitude winter/summer atmospheric profiles with various surface properties according to different land covers were defined. The IWAVE spectral response function (SRF) was interpolated at a 2.5 nm wavelength interval.

3.3. Cloud detection using threshold approach

In the same solar satellite viewing geometry, the reflectance values of clouds are often larger than the reflectance values of land or ocean. Cloud temperatures observed by satellite are often cooler than the underlying surface temperature. In this paper, a robustness and dynamic threshold method on MTSAT images was developed. According to the surface types and solar illuminations, different sets of threshold tests were applied on each pixel. When sun is above the horizon (e.g. solar elevation angle is higher than 3°), the bidirectional reflectance at 0.6 μm ($R_{0.6}$) was used to detect pixels containing cloud or snow.

The multispectral threshold identification method has been well-researched for determining the cloud mask. In this paper, new dynamic thresholds for visible wavelength and thresholds for both visible and infrared wavelengths based on monthly averaged values were proposed, for example the threshold test of $R_{0.6}$ implemented using dynamic thresholds. The threshold offsets were analyzed to ensure the actual threshold values have a large discrepancy between cloud-contaminated and cloud-free pixels. Land and water surfaces were applied with both proper surface RTM bidirectional reflectance distribution functions (BRDFs) and RTM simulations.

The simulation of cloud-free reflectance of each pixel was based on three-dimensional centroid-based interpolation method (Fig. 1). The apparent reflectance of clear-sky TOA is noted as P(X, Y, Z), where the X, Y, Z is the value of θ_{sun},θ_{sat}, α_{rel} as shown in Equation (2). x_1, x_2 are the x values difference between P(X,Y,Z) and p_1, p_2.

$$P(X,Y,Z) = \frac{1}{\Delta x\Delta y\Delta z}(x_2y_2z_2\Delta P_1 + x_1y_2z_2\Delta P_2 + x_1y_2z_1\Delta P_3 + x_2y_2z_1\Delta P_4 + x_2y_1z_2\Delta P_5 + x_1y_1z_2\Delta P_6 + x_1y_1z_1\Delta P_7 + x_2y_1z_1\Delta P_8) \quad (2)$$

The difference between eight points in the x, y, z direction are indicated as Δx, Δy, Δz, respectively, which are the step values of θ_{sun},θ_{sat}, α_{rel} ($\Delta x = x_1+x_2$, $\Delta y = y_1+y_2$, $\Delta z = z_1+z_2$).

The cloud mask algorithm contains a set of threshold tests where several criterions are tested together. If the pixel values of corrected reflectance and brightness temperature are similar to that of the threshold values, these pixels are considered as cloud contaminated areas with low confidence probability. After the determination of dynamic and static thresholds, threshold tests were implemented in order, as shown in Fig. 2. The annual average cloud cover probability over Hong Kong territory was then derived and illustrated in Fig. 3.

The cloud probability in Hong Kong shows a non-prominent spatial distribution varying from 0.58 to 0.62, generated from hourly geostationary satellite images of year 2012. The insignificant variation is mainly caused by: (i) low spatial resolution of geostationary MTSAT images (e.g. 4 km), where the Hong Kong territory has an area of 1104 km^2 but the areal resolution of satellite images is 16 km^2, thus the entire territory has only 69 pixels therefore some details or small clouds may be missed; and (ii) the geographic location of Hong Kong, where it is situated along a coastal region and is at sub-tropic climate zone, which is a cloud-prone area and the homogenous spatial patterns of cloud formation are expected.

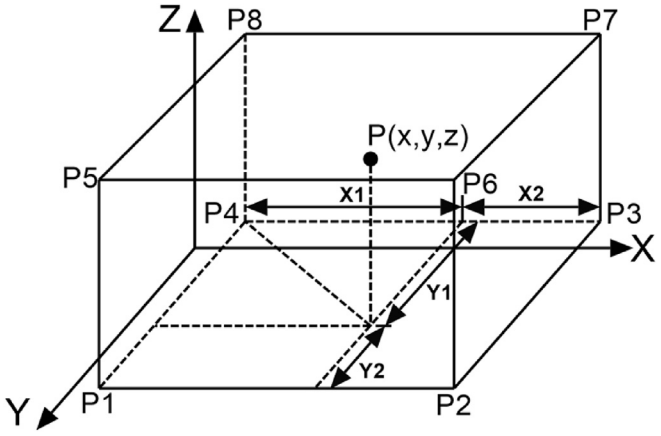

Fig. 1. Schematic representation of 3D centroid-based interpolation.

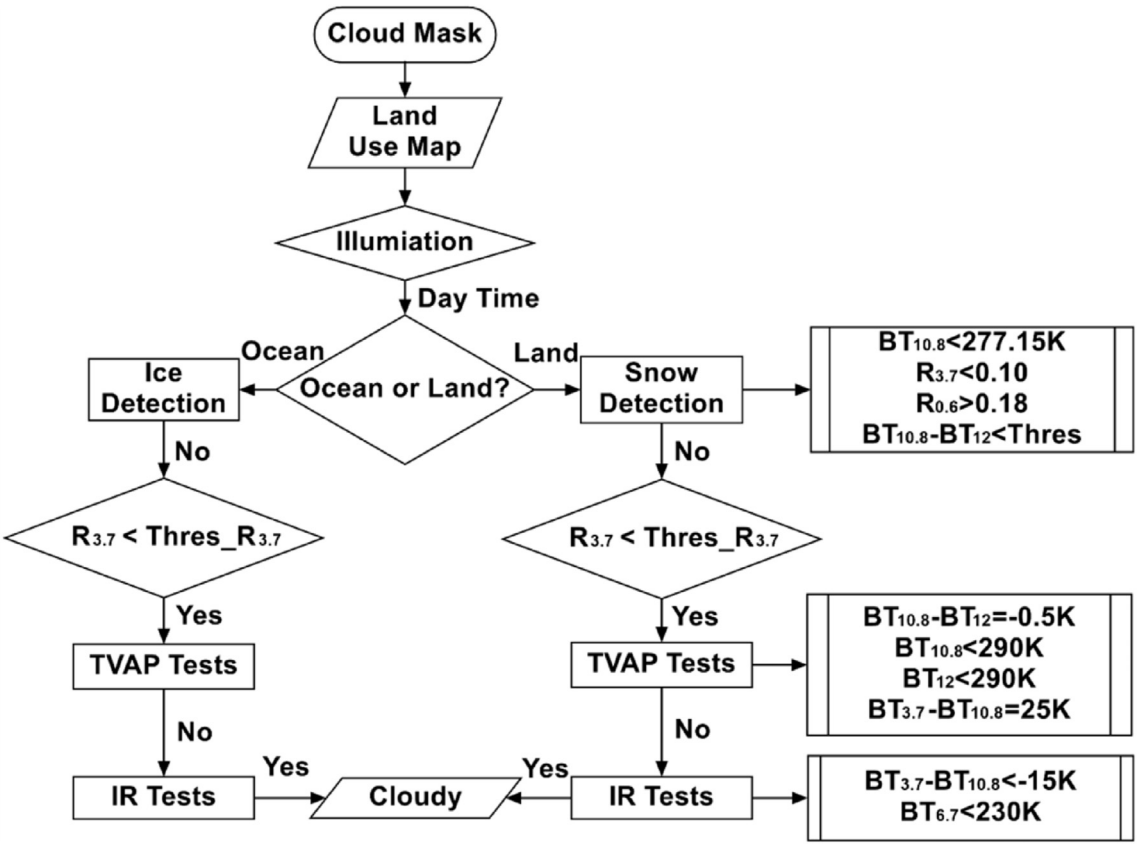

Fig. 2. Workflow for cloud detection approach.

4. Estimation of photovoltaic potential

A schematic diagram for calculating photovoltaic potential in Hong Kong on annual basis is presented in Fig. 4.

In this study, a 3 × 3 median convolution was applied to both DSM and DEM airborne LiDAR data [23]. The DSM was resized to a 3 m resolution and used for calculating solar radiation in Solar Analyst. Several criterions were applied to filter off unwanted pixels. After eliminating the ground pixels, barriers (buffer minus 1 m) on rooftops, shadows, and steep sloping pixels using decision tree classification, the optimal areas of rooftop pixels could be identified. The building polygons and solar radiation map were then spatially joined. It was assumed that at least two solar panels would be deployed in each candidate installation site; however polygons (sites) with areas smaller than 3 m^2 were then removed from the analysis. Finally, a territory-wide solar PV potential was derived as shown in Fig. 4.

4.1. Solar radiation modeling

A 3 × 3 median filter, used to remove the signal noise, was implemented using DSM and DEM airborne LiDAR data. The pixels were aggregated and the internal variation inside 3 × 3 kernels was reduced. This filtering process worked well on non-continuous data, such as edges of buildings which were not suitable for installing PV arrays. Since the size of entire Hong Kong DSM data is large and difficult to be processed in ArcGIS together at a single time, the DSM data were divided into four parts with 6 km overlapping areas in both easting and northing coordinates. And the resolution of the input DSM was downscaled to 3 m.

In the above sketch (Fig. 5), the CC part is the size of the input DSM, and the size of calculated solar radiation map should be the same as the input data. The latitude and longitude are automatically calculated from the input raster. Used in solar radiation calculations, the sky-size is defined as 200 cells per side for the resolution of the viewshed, sky map and sun map raster images. A raster sky representation is generated for both clear and obstructed views at a given location. The skymap is then estimated, with the viewshed in eight different directions, to determine the maximum angle of sky obstruction or horizon angle. The diffuse model type is the standard overcast sky. Since the results show that a non-prominent spatial variation of cloud covers presides over entire Hong Kong territories ranging from 0.58 to 0.62, the diffuse proportion and the transmissivity were calculated using the Hong Kong cloud coverage data from a station at the Hong Kong Observatory in year 2012. It is also assumed that a single set of equations for estimating the diffuse proportion and the transmissivity can be applied to the entire Hong Kong territories due to the insignificant spatial variation of cloud covers. The formulae are expressed as Equations (3) and (4):

$$T = 0.7\,P_{clear\ sky} + 0.5\,P_{partial\ cloudy} + 0.3\,P_{cloudy} \quad (3)$$

$$D = 0.2\,P_{clear\ sky} + 0.45\,P_{partial\ cloudy} + 0.7\,P_{cloudy} \quad (4)$$

where T is the transmissivity, D is the diffuse proportion, P_{clear} is the proportion of clear days, $P_{partialcloudy}$ is the proportion of partly cloudy days and P_{cloudy} is the proportion of cloudy days. A clear day is defined as 0–30% average percentage of cloud cover, partial cloudy day is 40%–70%, and cloudy is 80%–100% [24]. The weather data of 2012, including the cloud cover data, can be retrieved from the Hong Kong Observatory. Table 1 shows the computation of

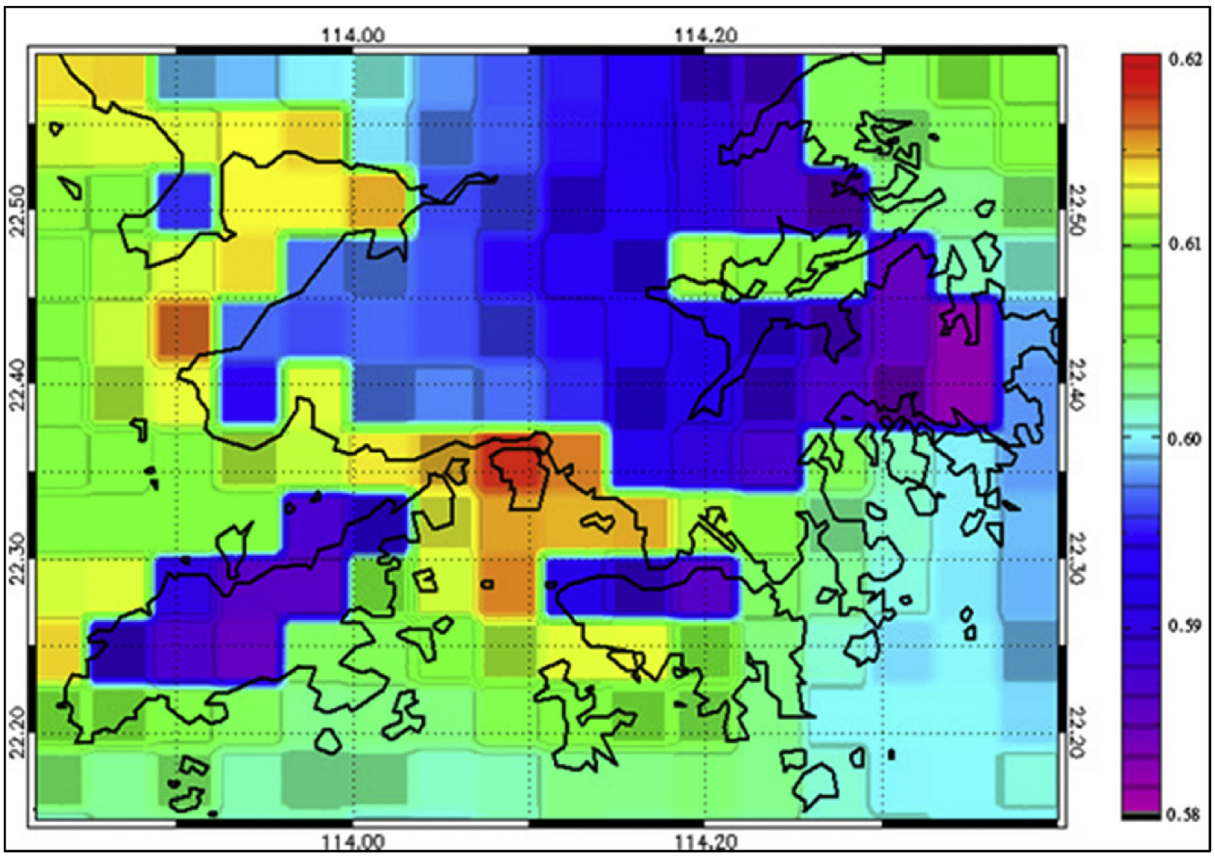

Fig. 3. Cloud probability map of Hong Kong.

diffuse proportion and transmissivity.

The average transmissivity and diffuse proportion in 2012 are T = 0.37 and D = 0.61 respectively. Compared to the default values of T_0 = 0.5 and D_0 = 0.3, the transmissivity is lower and diffuse proportion is higher. Solar analyst can simulate the solar radiation at any given time instant with a much higher spatial resolution (i.e. several meters) compared with NASA-SSE (i.e. results are 1° latitude by 1° longitude grid cells) and SolarGIS (i.e. original spatial resolution is about 3–5 km), which is essential to investigate solar radiation distribution in a micro-scale. The operation of Solar Analyst is time- and computer-demanding, taking around three days to complete the processing of one quarter of the data using a server computer.

The maximum annual solar radiation from the model outputs is about 2000 kWh/m^2, and the minimum value is 5 kWh/m^2. The mean annual value is 1497 kWh/m^2. According to the histogram analysis, about 40% of pixels are less than ca. 800 kWh/m^2. The value of 800 kWh/m^2 was observed as the first break value of five class classification using the Jenks Natural Breaks classification method. The obstruction from surrounding high-rise buildings may greatly affect the direct radiation on rooftops. The shadowing effect then becomes predominate. Considering the cost payback time and efficiency of solar panels, the pixels with values below the threshold (e.g. <800 kWh/m^2) were excluded.

4.2. Determination of PV potential on optimal building rooftops

There are several criteria for selecting the optimal locations of installing PV arrays. High resolution airborne LiDAR data were used to map the unused building rooftop areas. To acquire maximum amount of annual solar energy from solar irradiation, the most appropriate locations for installing solar panels were then selected. Compared to threshold-based filtering approaches, the hierarchy of decision tree classification was able to deliver the order of process and classification required for the different areas, which in this study was used to classify the rooftops appropriate for the deployment of PV arrays.

(1). Ground mask

A filtering of ground pixels was implemented based on the Object Height Model, created through the subtraction of DEM from DSM to eliminate the effects of the difference caused by different time frames of the airborne LiDAR data and building polygon shapefiles. The pixels with an object height below 2.5 m are considered as the ground pixels.

(2). Slope

The tilting of PV modules can be used to receive the maximum solar radiation and to avoid unwanted shading [25]. The residential PV systems are usually installed on sloped roofs while the commercial systems are installed on flat or low-slope rooftops [26]. However, some rooftops with steep slopes may lower the efficiency of electricity generation. The received solar radiation from PV modules decreases significantly, when the slopes exceed 40° [25]. It indicates that 40° is the maximum threshold for installing the PV modules. Thus, a slope calculation was processed using DSM data. Pixels with steep slopes would be excluded.

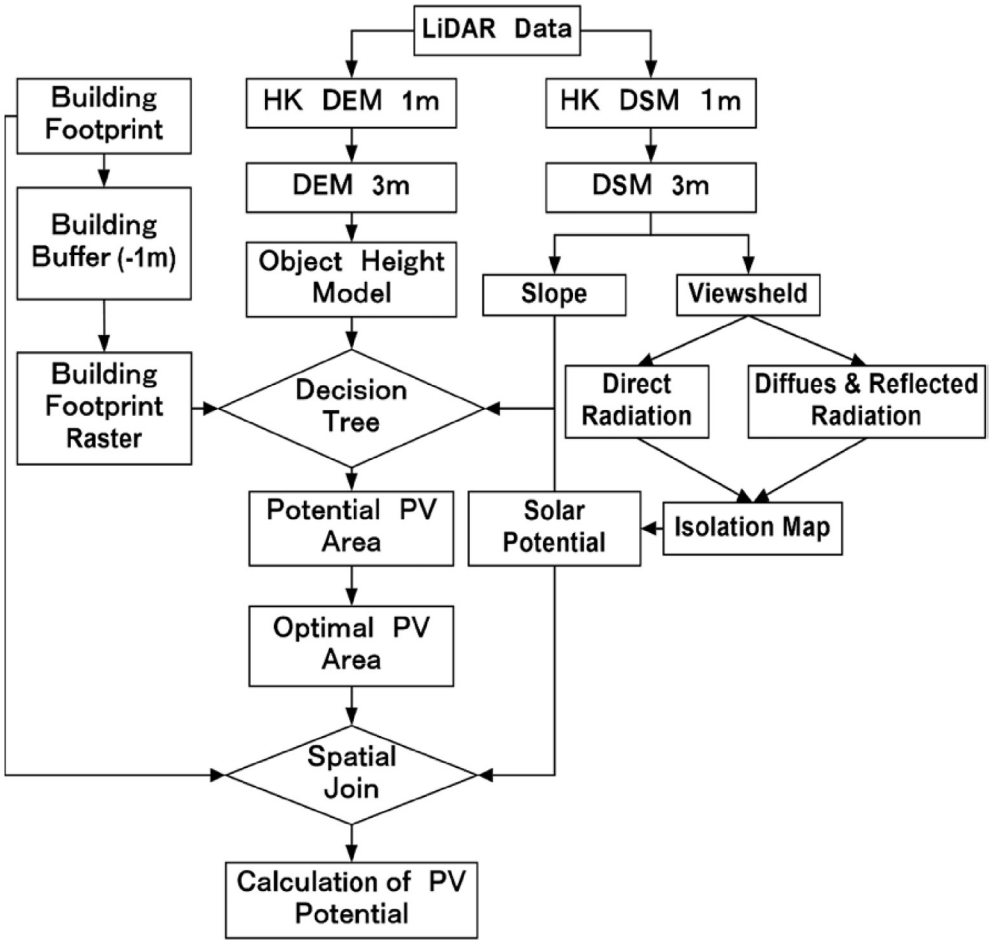

Fig. 4. Flow chart of the estimation of PV potential.

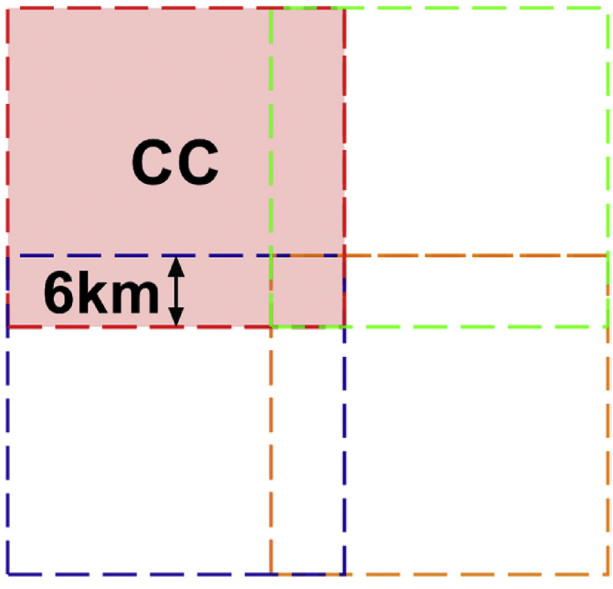

Fig. 5. Sketch of overlapping areas of solar radiation estimation.

(3). Barrier of building rooftop

Most of the building rooftops contain barriers which are not appropriate for installing PV modules. By applying a "minus 1 m" buffer areas, the edges of building footprints could then be filtered. The results can be converted into raster format for further processing.

(4). Shadow identification

In Hong Kong, shadowing effect from the nearby skyscrapers can greatly reduce the amount of solar electricity generation. Since the Solar Analyst accounts for the shadows cast by surrounding topography [15], a shadow detection algorithm can then be applied. The variation in solar radiation should then be taken into account on the topographic features and obstructions of the surrounding objects. If the value of solar radiation is lower than a certain threshold, it can be assumed that it is under shadows at the majority of the time. As the insolation map already takes into account of the aspect, slope, and viewshed of the topographic features, the threshold of lower values can then be used to filter off the pixels which are always covered by shadow. From the statistics of the solar radiation distribution, thresholds can be determined using the Jenks Natural Breaks method - those pixels with values lower than 800 kWh/m^2 are defined as shadow.

4.3. Estimating solar photovoltaic potential on rooftops

In Hong Kong, most of the rooftops of commercial and residential buildings are usually flat with bitumen surface. Therefore,

Table 1
Transmissivity and diffuse proportion of year 2012.

Month	No. of clear days	No. of partly cloudy days	No. of cloudy days	No. of days	Transmissivity	Diffuse proportion
Jan	0	9	22	31	0.358065	0.627419
Feb	0	2	27	29	0.313793	0.682759
Mar	3	6	22	31	0.377419	0.603226
Apr	0	5	25	30	0.333333	0.658333
May	0	6	25	31	0.33871	0.651613
Jun	0	6	24	30	0.34	0.65
Jul	0	14	17	31	0.390323	0.587097
Aug	0	12	19	31	0.377419	0.603226
Sep	3	14	13	30	0.433333	0.533333
Oct	2	20	9	31	0.454839	0.506452
Nov	0	10	20	30	0.366667	0.616667
Dec	1	9	21	31	0.370968	0.61129

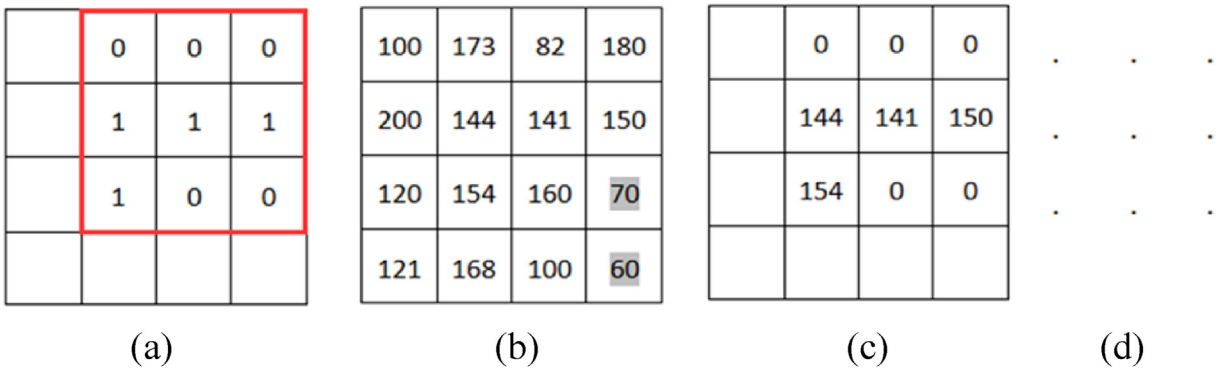

Fig. 6. Data conversion.

deployment of commercial rooftop PV system is more appropriate in Hong Kong. The PV panels are usually tilted at approximately latitude angle in order to maximize power production. In Hong Kong, this optimal tilting is around 14°–20° [27] to produce the maximum total power output and the south-facing orientation has a higher annual average insolation. The solar PV technologies are suitable for large-scale deployment and could be a significant source of renewable energy in Hong Kong [27].

The Photovoltaic Geographic Information System (PVGIS) database was then developed to estimate the potential solar electricity generation of the PV module at horizontal, vertical, and optimal inclination [28]. The following equation was applied for calculating the annual potential electricity generation E (unit: kWh) using defined module configuration and orientation [28]:

$$E = P_k \bullet P_R \bullet G_s \quad (5)$$

where P_k is the unit nominal power or the peak power in (kWp), P_R is the system performance ratio and G_s is the sum of global irradiation (kWh/m^2) on the surface yearly. The system performance ratio is a constant which describes the relationship between the actual power output and theoretical power output. The performance ratio may vary as the external environment changes. For example, a rise in temperature will decrease the performance ratio. A typical value of 0.75 is assumed for the roof mounted system with modules from mono- or poly-crystalline silicon type [28]. The size of the systems is measured in nominal power (Wp) which represents the maximum power output of PV modules at Standard Test Conditions (STC) [28]. The nominal plant energy output of a PV plant can be calculated using Equation (6) [29]:

$$E_n = G_a \bullet A \bullet \eta \quad (6)$$

where E_n is the nominal plant energy output (kWh), G_a is the average solar radiation intensity (kWh/m^2) in a certain period of time per unit area, A is the generator area (m^2) of the PV plant and η is the efficiency factor of the PV modules. The factor of nominal power divided by the incident light intensity is the module efficiency which is the ratio of electrical output from light energy. The above nominal plant power output assumes that the performance ratio is 100%. However, the actual output is not the same due to the lumped contribution of the sources of performance loss. The actual energy output can be calculated using Equation (7) [29]:

$$E_{out} = E_n \bullet P_R = G_a \bullet A \bullet \eta \bullet PR \quad (7)$$

where E_{out} is the electrical energy output by the PV plant and PR is the system performance ratio. The typical value of 0.75 for the performance ratio of crystalline silicon type of PV module was adopted in this study. The efficiency of standard crystalline silicon module is about 17%. The annual insolation map produced by the Solar Analyst could be used as the input of the annual sum of global irradiation (kWh/m^2). The PV potential based on each building was then calculated in the GIS platform.

4.4. Data conversion

Each pixel in the raster image was converted into a point with insolation value. The points falling outside the area of optimal PV polygon were filtered off. The output of decision tree is a binary raster image, where “1” indicates an appropriate area and “0” indicates a filtered area. The output raster was then multiplied with the solar radiation output data to estimate the solar radiation of unused areas. These solar radiation pixel values were converted from raster into the point, such as illustrated in Fig. 6.

In Fig. 6 above, the red rectangles (a) indicates the output

building area after decision tree classification; (b) is the estimated solar radiation value with unit of kilowatt hour per square meter (kWh/m^2); (c) is the result from raster calculator, using (a) multiply by (b); and (d) is the conversion from raster map (c) into point. It was observed that there are 2 pixel values smaller than the defined threshold, and these pixels would be excluded. There are 9 points in total, but only 4 values are above 0. In this example, the total potential solar radiation on rooftop area is the sum of estimated solar radiation in Fig. 6(c) and is equal to 589 kWh/m^2 if the solar photovoltaic arrays are only installed on the appropriate areas.

In this study, there are a total of 29,743,281 points and among them, 10,660,310 have null value. It indicates that around 1/3 rooftop pixels of Hong Kong buildings are unsuitable for installation of solar photovoltaic modules. After converting the raster image into point data, spatial join was performed to estimate the efficiency and total electricity generation in each building.

Spatial join is a function of joining attributes from one feature to another according to the spatial relationship [30]. The polygons of optimal PV areas and the insolation points were spatially joined into building polygons. The sum of optimal PV areas and average solar radiation of each building were calculated if the points completely fall inside the building footprints.

5. Results and discussion

5.1. Validation of the developed methodology

The proposed methodology was validated through the direct comparison with MODIS cloud mask products MOD06 observed between 2 a.m. and 3 a.m. GMT time. MODIS instrument with 36 channels provides a higher spatial (1 km) and higher spectral resolution from the shortwave visible to the longwave infrared spectrum. The comparison was conducted on a pixel by pixel basis. A temporal matching criterion is ±5 min between the MODIS and MTSAT measurements. Results show that the lowest and highest success ratios of validation dataset are 0.84 and 0.97, respectively. These success ratios indicate that high degree of consistency of cloud detection between the MTSAT and MODIS MOD06 products.

5.2. Validation with ground-based solar radiation observation

To validate the solar radiation simulation model, pyranometers with sensitivity of about 7 μV/(W/m^2) have been set on the rooftop of the Hong Kong Polytechnic University (Fig. 7) to measure direct and diffuse solar radiation continuously between November and December 2012. Result shows that a value of 140 kWh/m^2 compared with simulated 152 kWh/m^2 suggesting about 91.4% accuracy for the model.

5.3. Results

The estimated solar photovoltaic potential of rooftops in Tsim Sha Tsui, Kowloon peninsula is illustrated as an example in Fig. 7. Hong Kong contains about 309,606 buildings, 239,833 buildings are suitable for solar panel installation. The sum of PV potential is about 2.66 TWh. However, the mean potential PV per building is only about 11.094 MWh. A map accounting for the percentage of optimal PV area divided by the total rooftop area is illustrated in Fig. 8. This map shows the feasibility of the PV system installed on individual buildings. It is also observed that large buildings have a larger percentage of PV deployment than the smaller ones. Considering certain areas on the rooftops are not appropriate for the deployment of solar panels due to the all-year-round shadows caused by surrounding high-rise buildings and walls, and the necessary space between panels, the utilization rate is calculated to indicate areas that can be used for each rooftop. In Fig. 9, about 10% of buildings have utilization rate below 40%, most of which are residential buildings.

The total and average PV potentials in the residential regions are larger than that of the commercial region. It indicates that the efficiency and total electricity generation in the residential areas are higher than the commercial areas. However, it is observed that the efficiency of residential buildings in commercial areas is lower than the commercial buildings in the same areas that contain larger rooftops, which is mainly due to lots of skyscrapers in commercial districts. The skyscrapers obstruct the viewshed of the low-rise buildings, therefore, the solar radiation incident on the PV is greatly reduced. In the residential areas, the buildings are spatially distributed and discrete. It greatly reduces the chance of obstruction by surrounding buildings. Some buildings, especially for the village houses, are low-rising and have better viewsheds. A better viewshed gives a higher efficiency in generation of electricity.

The residential buildings have the lowest utilization rate but industrial buildings have the greatest utilization rate. The industrial buildings are usually located at lower building density districts and with larger rooftop areas. As a result, the PV systems on industrial rooftops can generate electricity with a higher efficiency.

Fig. 7. Location and layout of the auxiliary instruments.

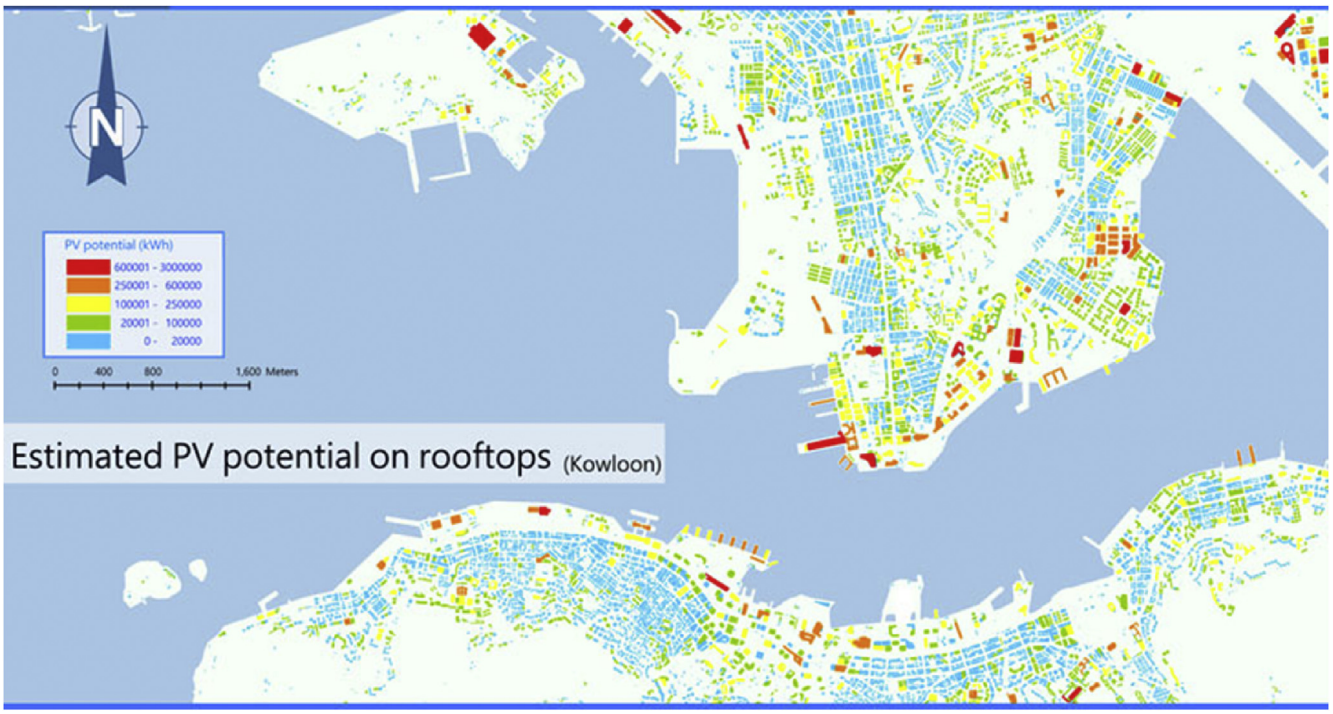

Fig. 8. Estimated solar photovoltaic potential on rooftops over Kowloon peninsula and northern part of Hong Kong Island.

5.4. Limitations in data processing

(1). Sources from different datasets

Different resolutions of data sources have long been a challenge in data processing. In this study, the resolutions of DEM and DSM are resampled at 3 m resolution. GIS data including the land use map and building footprints are in vector files. The different resolutions between the DEM/DSM, and land use map results in positional displacement. The time of acquisition between LiDAR data and GIS data are also different.

In addition, from the results of decision tree, it was observed that the utilization rates of large buildings are higher than small buildings. This is mainly due to the pixels from small buildings

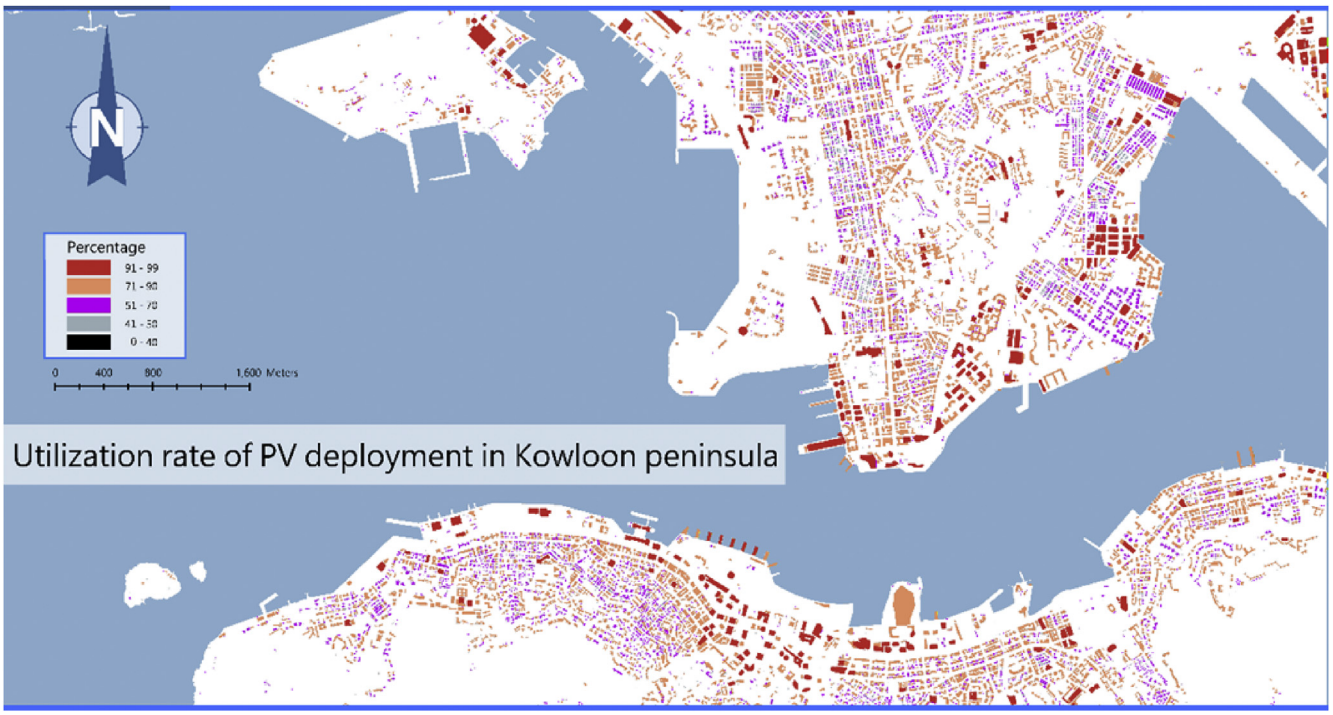

Fig. 9. Utilization rate of PV deployment in Kowloon peninsula and northern part of Hong Kong Island.

being already filtered by the potential barriers or other obstacles. The inconsistencies between building polygons and LiDAR data would pose variability to the potential areas. Although the mismatching areas are small in this study, the total number of small buildings is greater than that of large buildings in Hong Kong. Thus, the estimated PV potentials in residential buildings, which usually contain smaller rooftop areas, may be underestimated.

(2). Off-terrain points in Digital Terrain Model

Buildings may be misclassified as the ground features from the decision tree classification process, which could be due to the height information of some off-terrain points, e.g. buildings, which may have been misclassified in both DSM and DEM data. The classifier might not be able to accurately distinguish between the terrain points and off-terrain points for complex topographic features. The off-terrain point results in a zero value of object height model and thus the node "height above 2.5 m" may misclassify the buildings as ground features.

(3). Timeliness of the data

Another error may occur from the GIS data. As the GIS data used in this study are not as up-to-date as the airborne LiDAR data, some newer buildings were not included in the calculation whereas some demolished buildings might still exist in the GIS data but not in the LiDAR. This type of error can be corrected through the ground filtering in decision tree classification. Due to the fact that the information of new buildings has not been included in this study, the PV potential may thus be underestimated.

6. Conclusion

Greenhouse gases accelerate the insulating effect in atmosphere and global warming. Adopting solar photovoltaic technology is one way to use renewable resources to mitigate the climatic change. In Hong Kong, the solar energy contributes only 1.5% of total renewable energy usage in 2012. This study estimated the annual PV potential of Hong Kong considering the influences of cloud covers, and natural and artificial geomorphology in the solar radiation estimation. The optimal areas to deploy PV panels were identified on unused building rooftops based on a set of decision tree criteria. The summarization of PV potential for the optimal rooftops is 2.66 TWh.

This study was the first ever to derive a cloud cover probability map over the entire Hong Kong territories using geostationary satellite images, which are vital for cloud detection and cloud movement tracking. Although the spatial resolution at 4 km may not be sufficient for detailed depictions over territories, it is still a promising measure with its high temporal resolution (e.g. 1 h resolution). A non-prominent spatial distribution of cloud probability in Hong Kong was observed, thus only a single set of equations for estimating the diffuse proportion and the transmissivity in the solar radiation model can be applied to the entire territory due to the insignificant spatial variation of cloud covers.

Results of solar potentials in Hong Kong are promising. This study has developed a robust and accurate method for estimating the optimal PV potential on building rooftops in the entire city of Hong Kong. The developed methodology can be applied to other places to study the application of PV modules in order to promote and encourage the use of solar energy.

Acknowledgments

This research was sponsored by the Public Policy Research Funding (2013.A6.024.13A) from the Central Policy Unit, the Government of the Hong Kong Special Administrative Region. The authors would like to thank the Hong Kong Observatory for the MTSAT images and climate data, the Hong Kong Planning Department for the land use and land cover map, Hong Kong Lands Department for building GIS data, and the Hong Kong Civil Engineering and Development Department for airborne LiDAR data.

References

[1] EMSD, Hong Kong Energy End-use Data 14 (2014). Retrieved July 31, 2015 from, http://www.emsd.gov.hk/filemanager/en/content_762/HKEEUD2014.pdf.
[2] Intergovernmental Panel on Climate Change (IPCC), Climate Change 2007: Synthesis Report, Summary for Policymakers, 2007. Retrieved July 31, 2015 from https://www.ipcc.ch/pdf/assessment-report/ar4/syr/ar4_syr_spm.pdf.
[3] EMSD, Study on the Potential Applications of Renewable Energy in Hong Kong 9 (2002). Retrieved July 11, 2016 from, http://www.emsd.gov.hk/filemanager/en/content_299/stage1_report.pdf.
[4] EMSD, Hong Kong Energy End-use Data 2013 53 (2013). Retrieved July 31, 2015 from http://www.emsd.gov.hk/emsd/e_download/pee/HKEEUD2013.pdf.
[5] J.M. Pearce, Photovoltaics – a path to sustainable futures, Futures 34 (7) (2002) 663–674.
[6] J. Hofierka, M. Šúri, The solar radiation model for Open source GIS: implementation and applications, in: Proceedings of Open Source GIS - GRASS Users Conference, 2002.
[7] A. Jochem, B. Höfle, M. Rutzinger, N. Pfeifer, Automatic roof plane detection and analysis in airborne LiDAR point clouds for solar potential assessment, Sensors 9 (2009) 5241–5262.
[8] M. Šúri, A. Thomas, T.A. Huld, E.D. Dunlop, PV-GIS: a web-based solar radiation database for the calculation of PV potential in Europe, Int. J. Sustain. Energy 24 (2) (2005) 55–67.
[9] N. Lukač, S. Seme, D. Žlaus, G. Štumberger, B. Žalik, Buildings roofs photovoltaic potential assessment based on LiDAR (Light Detection and Ranging) data, Energy 66 (2014) 598–609.
[10] H.T. Nguyen, J.M. Pearce, R. Harrap, G. Barber, The application of LiDAR to assessment of rooftop solar photovoltaic deployment potential in a municipal district unit, Sensors 12 (2012) 4534–4558.
[11] H.T. Nguyen, J.M. Pearce, Incorporating shading losses in solar photovoltaic potential assessment at the municipal scale, Sol. Energy 86 (2012) 1245–1260.
[12] R. Dubayah, P.M. Rich, Topographic solar radiation models for GIS, Int. J. Geogr. Inf. Syst. 9 (1995) 405–419.
[13] I. Mészáros, P. Miklánek, J. Parajka, Solar energy income modelling in mountainous areas, in: ERB and Northern European FRIEND Project 5 Conference, Demänovskádolina, Slovakia, 2002, 1998.
[14] M. Šúri, J. Hofierka, A new GIS-based solar radiation model and its application to photovoltaic assessments, Trans. GIS 8 (2) (2004) 175–190.
[15] P. Fu, P.M. Rich, Sol. Analyst 1.0 User Man. (2000). Retrieved July 31, 2015 from https://www.sciencebase.gov/catalog/item/5140acafe4b089809dbf56f5.
[16] P.M. Rich, A Manual for Analysis of Hemispherical Canopy Photography, Los Alamos National Laboratory Report, 1989. LA–11733–M.
[17] P.M. Rich, Characterizing plant canopies with hemispherical photography, Remote Sens. Rev. 5 (1990) 13–29.
[18] Census and Statistics Department, Summary results of population census, 2011. Retrieved August 8, 2013 from http://www.census2011.gov.hk/pdf/summary-results.pdf.
[19] EMSD, Hong Kong Energy End-use Data 2015 13 (2015). Retrieved July 11, 2016 from, http://www.emsd.gov.hk/filemanager/en/content_762/HKEEUD2015.pdf.
[20] C.S. Lai, C.T. So, K.C. Ng, D. Jonas, The Territory – Wide Airborne Light Detection and Ranging Survey for the Hong Kong Special Administrative Region, 2012. Retrieved Apr 27 2016 from http://www.aamgroup.com/_literature_112830/LiDAR_Survey_for_the_Hong_Kong_Special_Administrative_Region.
[21] Hong Kong Observatory, The Year's Weather – 2012, 2012. Retrieved Apr 27 2016 from http://www.hko.gov.hk/wxinfo/pastwx/ywx2012.htm.
[22] E.F. Vertmote, D. Tanré, J.L. Deuzé, M. Herman, J. Morcrette, Second simulation of the satellite signal in the solar Spectrum, 6S: an overview, Trans. Geoscience Remote Sens. 35 (3) (1997) 675–686.
[23] R.A.A. Nobrega, J.A. Quintanilha, C.G. O'Hara, A Noise-removal Approach for LiDAR Intensity Images Using Anisotropic Diffusion Filtering to Preserve Object Shape Characteristics, 2007. Retrieved Apr 27 2016 from http://www.asprs.org/wp-content/uploads/2011/01/0049.pdf.
[24] ESRI, An overview of the Solar Radiation tools (2016). Retrieved July 11, 2016 from, http://desktop.arcgis.com/en/arcmap/10.3/tools/spatial-analyst-toolbox/an-overview-of-the-solar-radiation-tools.htm.
[25] H.X. Yang, L. Lu, The optimum tilt angles and orientations of PV claddings for building-integrated photovoltaic (bipv) applications, J. Sol. Energy Eng. 129 (2007) 253–255.
[26] A. Goodrich, T. James, M. Woodhouse, Residential, Commercial, and Utility-

scale Photovoltaic (PV) System Prices in the United States: Current Drivers and Cost-reduction Opportunities, 2012.
[27] EMSD, Study on the Potential Applications of Renewable Energy in Hong Kong Stage 1 Study Report, Electrical and Mechanical Services Department, 2002. Retrieved July 31, 2015 from http://www.emsd.gov.hk/emsd/e_download/wnew/stage1_report.pdf.
[28] M. Šúri, A. Thomas, T.A. Huld, E.D. Dunlop, PV-GIS: a web-based solar radiation database for the calculation of PV potential in Europe, Int. J. Sustain. Energy 24 (2) (2005) 55–67.
[29] SMA Solar Technology AG, Performance Ratio Quality Factor for the PV Plant, 2010. Retrieved July 31, 2015 from http://files.sma.de/dl/7680/Perfratio-UEN100810.pdf.
[30] ESRI, ArcGIS Help 10.1 Spat. Join. Anal. (2013). Retrieved July 31, 2015 from http://resources.arcgis.com/en/help/main/10.1/index.html#//000800000000q000000.